ELSEVIER

International Journal of Mass Spectrometry 223–224 (2003) 21–36

International Journal of Mass Spectrometry

www.elsevier.com/locate/ijms

Edge plasma-relevant ion–surface collision processes

S. Cernusca [a], HP. Winter [a], F. Aumayr [a,*], A. Qayyum [b], W. Schustereder [b], C. Mair [b], P. Scheier [b], T.D. Märk [b,1]

[a] *Institut für Allgemeine Physik, TU Wien, Wiedner Hauptstr. 8-10, A-1040 Wien, Austria*
[b] *Institut für Ionenphysik, Universität Innsbruck, Technikerstr. 25, A-6020 Innsbruck, Austria*

Received 27 November 2001; accepted 4 February 2002

Abstract

Graphite tiles or carbon-coated structures are largely used as wall or divertor materials in magnetically confined fusion devices. Laboratory work on plasma–wall interaction has so far mainly focused on obtaining physical and chemical sputtering yields for such materials. Much less is known on electron emission and molecular fragmentation and reactions during ion impact on graphite surfaces, despite the fact that both processes might play a decisive role in plasma–wall interaction. We therefore have measured such data for fusion-relevant ion species (e.g., H_n^+, $n = 1$–3 and C^{z+}, $z = 1, 2, 4, 5$) in the eV to keV impact energy region typical for fusion edge plasma conditions. As a target surface graphite tiles from the Tokamak experiment Tore Supra in CEA-Cadarache/France have been used. Implications of the experimental results for plasma edge modeling are also discussed. (Int J Mass Spectrom 223–224 (2003) 21–36)

PACS: 34.50.Dy; 79.20.Rf

Keywords: Plasma–surface interaction; Graphite; Multiply charged ion

1. Introduction

The understanding and control of plasma–surface interaction (PSI) is not only of great importance for the plasma processing industry, but also rather critical for the future success of fusion energy development [1]. While in early fusion devices the energy content was largely insufficient to destroy the plasma-facing materials, it has nowadays reached such high levels that divertor design including appropriate material selection has become very important for next-step fusion machines (in particular, ITER-FEAT). Interaction with the wall material largely influences the performance of magnetically confined plasmas. The use of low Z materials such as carbon, boron and beryllium has been a great success in the present large Tokamaks [2]. In ITER design, graphite-based low Z material is recommended for divertor plates and first wall protection for the initial operation phase in order to minimize the risk of plasma contamination.

The available databases on PSI mainly include data on physical and chemical sputtering/erosion, material deposition and hydrogen/deuterium recycling. Much less reliable data are known for electron emission from wall materials under impact of energetic ions, atoms or electrons [3] and data on molecular fragmentation

* Corresponding author. E-mail: aumayr@iap.tuwien.ac.at
[1] Also adjunct professor at Department of Plasmaphysics, Comenius University, Bratislava SK-84248, Slovak Republic.

1387-3806/02/$ – see front matter
PII S1387-3806(02)00777-7

during molecular ion scattering are practically non-existing [4]. The latter have so far been limited to laboratory studies mainly involving H^+ and O^+ projectiles [5] and only recently extended to systems such as CH_3^+ and CH_4^+ but with conflicting results [6,7]. However, electron emission can play an important role in PSI by influencing the boundary plasma (e.g., via the sheath potential) and the intensity of plasma–wall interaction accordingly. Basically, a large yield of emitted electrons is expected to reduce the sheath potential. This in turn reduces the impact energy of ions and consequently the ion flux to the surface and the related sputtering yield. Molecular fragmentation and reactive collisions, on the other hand, may significantly change the ion and neutral composition in the plasma edge due to the emission of neutrals and ions not present in the plasma prior to the impact and thus change its properties drastically.

Recent studies in the field of thermonuclear fusion based on the magnetic confinement of high temperature plasma have demonstrated that the conditions at the plasma periphery ("plasma edge") play an important role for achieving, sustaining and controlling the thermonuclear fusion plasma [4,8]. In order to understand and elucidate the role of the radiative and collisional processes in this plasma edge region (in particular, their (i) influence on the plasma properties and dynamics and their (ii) use for controlling the plasma conditions), it is essential to have available a detailed and quantitative knowledge on (i) these elementary processes in the gas phase [8] (such as cross sections, reaction rate coefficients, etc.) and on (ii) the interaction of the gas phase particles with the plasma walls [4]. These data are necessary as input for edge plasma modeling and various diagnostic techniques.

In view of the lack of available data, the main objective of this paper is to present measured data for fusion-relevant ion species (e.g., H_n^+, $n = 1$–3) in the eV to keV impact energy region typical for fusion edge plasma conditions. As for the target surface, graphite tiles from the Tokamak experiment Tore Supra in CEA-Cadarache/France have been used. Implications of the experimental results for plasma edge modeling are also discussed.

2. Ion-induced electron emission from carbon surfaces

2.1. Mechanisms of ion-induced electron emission

In a simple approach ion-induced electron emission can result from the kinetic (kinetic emission—KE) as well as the potential energy (potential emission—PE) of the projectile ions. KE requires a certain impact velocity threshold whereas PE only needs a minimum potential energy deposited upon impact, i.e., a total ion recombination energy surpassing twice the surface work function W_ϕ. There are several ways in which slow ions can excite electrons at the expense of their kinetic energy. The two most prominent mechanisms involve direct binary collisions with target electrons and electron promotion in quasi-molecular collisions of projectile ions with target atom cores. The latter process strongly depends on details of the electronic structure of projectile and target atoms. The situation is further complicated by the fact that the amount of electrons emitted not only depends on the primary electron excitation mechanism but also on other properties of the solid surface, e.g., the mean free path for low energy electrons inside the target bulk and their escape probability through the surface barrier [9].

In a series of recent studies for clean gold surfaces we have tried to disentangle some of these contributions to the total electron yield. With very slow ions in higher charge states the domain of exclusive PE can be investigated [10,11]. Coincidence measurements between emitted electrons and projectiles scattered under grazing angles from a monocrystalline surface can separate the PE and KE contributions [12]. Exclusive KE mechanisms have been studied at the KE velocity threshold for various singly charged ions on polycrystalline Au [13].

In this chapter we present measured total electron yields for singly and multiply charged (atomic) ion impact on graphite surfaces. On the one hand, graphite is quite similar to the gold target used in our previous studies: both target materials are good conductors and the work function is almost the same (5.1 eV for gold and 5.0 eV for graphite). On the other hand, their Fermi

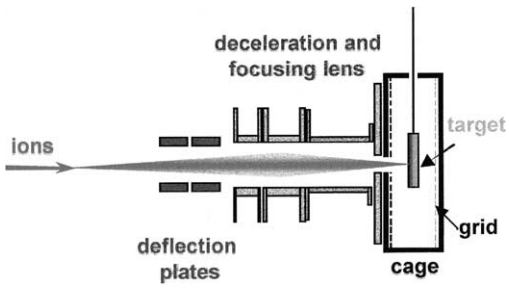

Fig. 1. Experimental set-up.

energies (approximately 7.6 eV for gold [14,15] and 21.3 eV for graphite [16]) are quite different and this difference might therefore become apparent from a direct comparison of the two targets.

2.2. Experimental set-up and technique

As projectiles for our studies we have used singly and multiply charged ions (MCIs) characteristic for a typical edge plasma, namely H^+, H_2^+, H_3^+, C^{q+}, N^+ and O^+. These ions have been produced in our 5 GHz ECR ion source [17], extracted and accelerated with a few keV, formed to a beam, mass-to-charge separated in a sector magnet and directed onto the carbon target situated in an UHV chamber. To obtain impact energies typical for the plasma edge (several eV to several keV), the ions were decelerated in front of the target by means of a deceleration and focusing lens (Fig. 1).

Total electron yields γ were determined by means of current measurements for impinging ions and emitted electrons [18] (see Figs. 2 and 3) and resulting total errors can be estimated to about ±7%. Data were obtained for normally incident ions only.

2.3. Graphite targets

For our experiments we have received carbon tiles from Association EURATOM—CEA/Cadarache which were used there as limiter material in Tore Supra. The surface orientations of these carbon compound tiles exhibit different thermal conductivity (two high and one low thermal conductivity sides, see Fig. 4).

Since the electron transport in a conductor is connected to its thermal conductivity, some influence of thermal conductivity on the total electron yield can be expected. Consequently, we have investigated electron emission from the high (HC1 and HC2) and low (LC) thermal conductivity sides separately. In addition, for comparison we have investigated a highly oriented pyrolytic graphite (HOPG) sample, constituting a standard material in surface science.

Before taking data all targets have been sputter-cleaned by impact of 3 keV Ar^+ ions and all investigations were carried out under ultra-high-vacuum (UHV) conditions (typically 10^{-10} mbar). Carbon surfaces inside a fusion device are supposed to be dynamically clean due to heavy bombardment by the plasma particles.

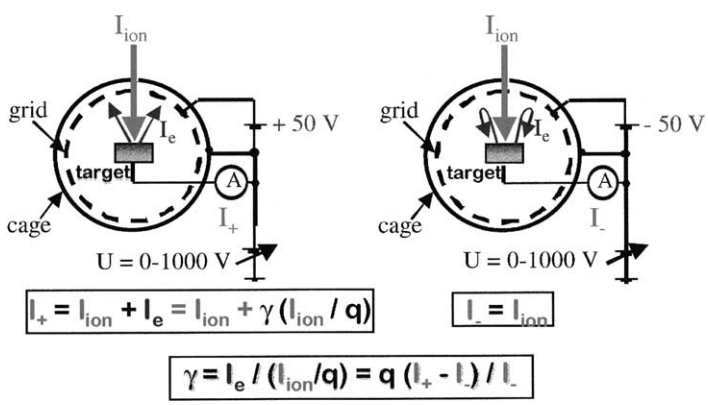

Fig. 2. Determination of total electron yields by measuring the currents of incoming ions and emitted electrons.

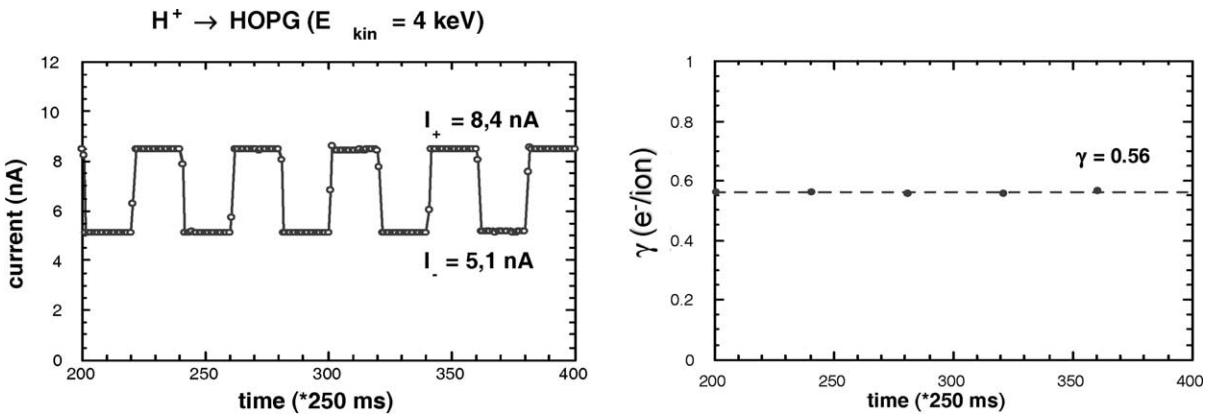

Fig. 3. Raw data as obtained for impact of H^+ on a graphite (HOPG) target.

2.4. Results for singly charged projectiles

Fig. 5 shows measured total electron yields γ induced by impact of H^+, H_2^+, H_3^+, C^+, N^+ and O^+ ions on the different carbon surfaces (C_L and C_H denote results for the low- and high-conductivity sides of the carbon tiles, HOPG denotes the highly oriented pyrolytic graphite sample). As a general trend, about 20% less electrons are emitted from the high conductivity side of the carbon tiles as compared to the low conductivity side (both high conductivity sides denoted as C_{H1} and C_{H2} yield identical results within our error limits, as shown for the case of H_2^+ impact in Fig. 5), whereas results for HOPG are generally situated between the results for C_L and C_H. For all projectile species electron emission starts around an ion impact velocity threshold of 10^5 m/s, corresponding to an impact energy (per atomic mass unit) of 50 eV/amu.

Only for the hydrogen ions can data be compared to literature results. Our data are in very good agreement with measurements performed on bulk carbon samples by Large and Whitlock [19] and Cawthron [20], and somewhat lower than data obtained on self supporting carbon foils [21]. To our knowledge no data for the other systems are available so far.

Electron yields as measured for the same projectile ions on clean polycrystalline gold [22] are shown in Figs. 6 and 7 and compared to the HOPG results. At projectile velocities below approximately 8×10^5 m/s the yields decrease linearly with the projectile velocity. If one extrapolates this trend to zero yield, the resulting intersection with the velocity-axis appears at around 1×10^5 m/s in the case of our carbon target, which is considerably lower than the value obtained for Au (3.5×10^5 m/s) [22].

Although we did not perform measurements with fast neutral hydrogen atoms on graphite, we can

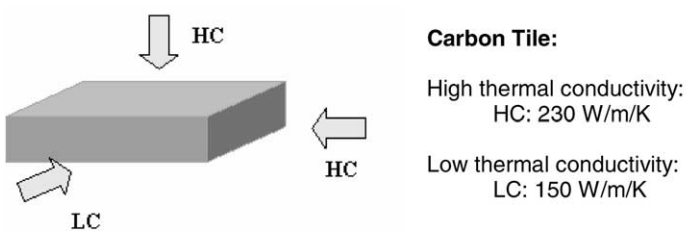

Fig. 4. Carbon tiles from Tore Supra (which exhibit surface orientations with different thermal conductivity) have been used as a target material together with HOPG.

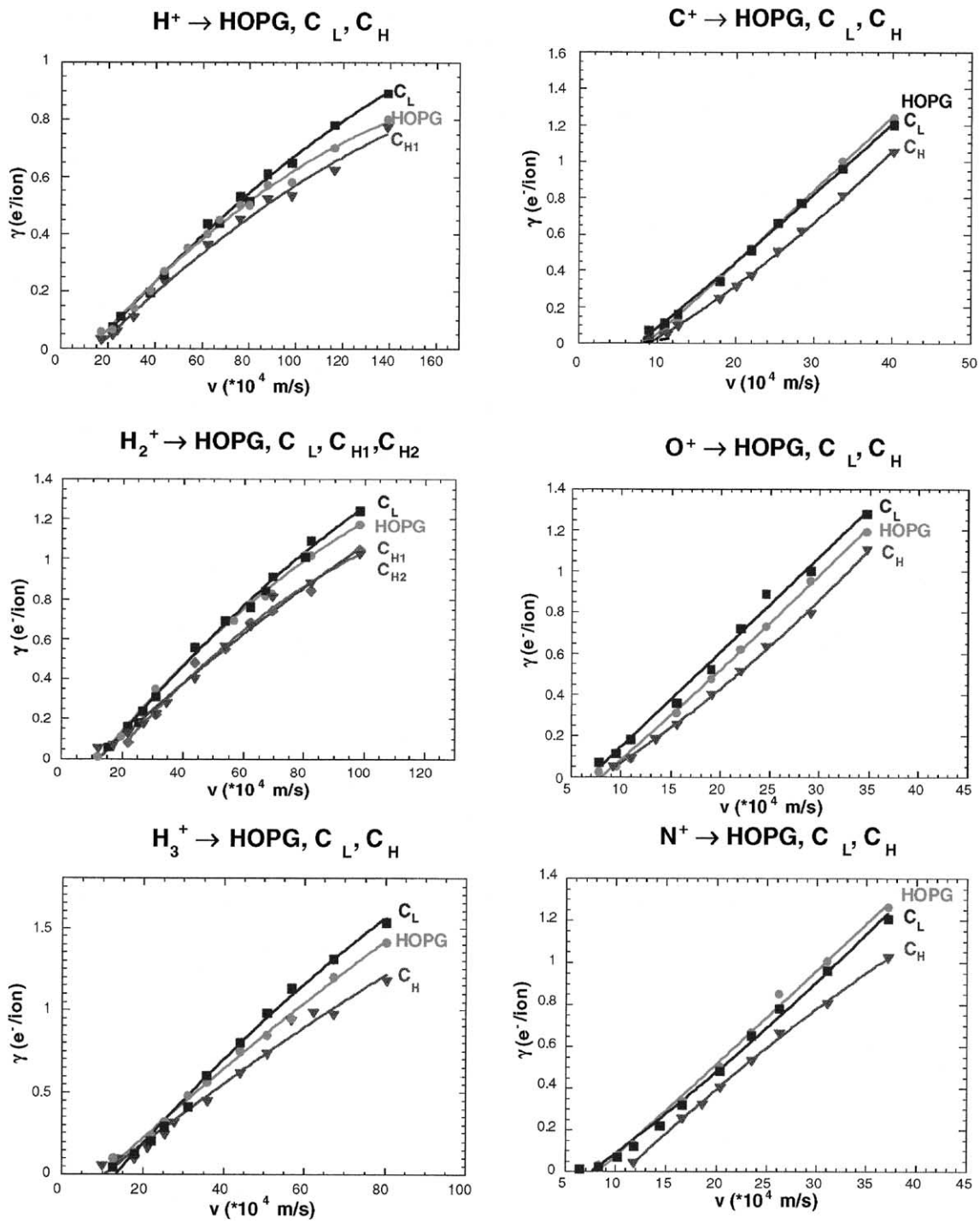

Fig. 5. Total electron yields vs. impact velocity v for impact of H^+, H_2^+, H_3^+, C^+, N^+ and O^+ ions on different carbon tile surfaces (see text).

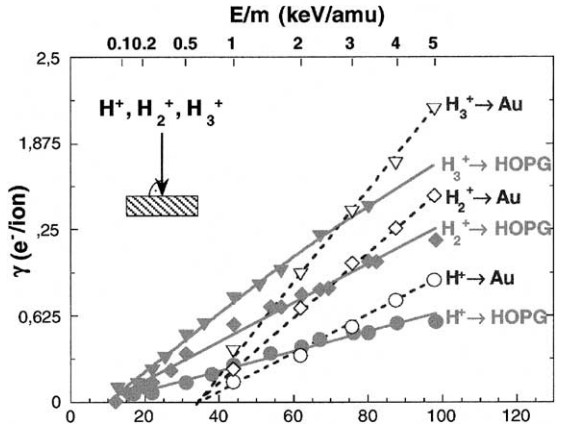

Fig. 6. Comparison between total electron yields vs. impact velocity v for impact of H^+, H_2^+, H_3^+ on HOPG and Au, respectively.

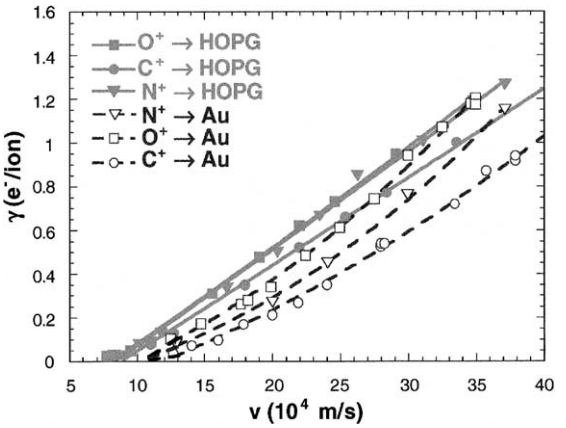

Fig. 7. Comparison between total electron yields vs. impact velocity v for impact of C^+, N^+, O^+ on HOPG and Au, respectively.

evaluate a hypothetical H^0-yield under the assumption that the relation for equally fast ions:

$$\gamma(H_n{}^+) = \gamma(H^+) + (n-1)\gamma(H^0) \quad (1)$$

holds for graphite in the same way as for the Au target [22], and therefore we should obtain:

$$\gamma(H^0) = \frac{\gamma(H_n{}^+) - \gamma(H^+)}{n-1} \quad (2)$$

Values for $\gamma(H^0)$ derived in this way are shown in Fig. 8 together with measured yields (in electrons per proton) for the various hydrogen ions as a function of the number of projectile screening electrons. Within the combined error bars (±10%) the $\gamma(H^0)$ values calculated according to Eq. (2) from data for protons and $H_2{}^+$ agree with values derived from yields for protons and $H_3{}^+$, respectively. This agreement gives

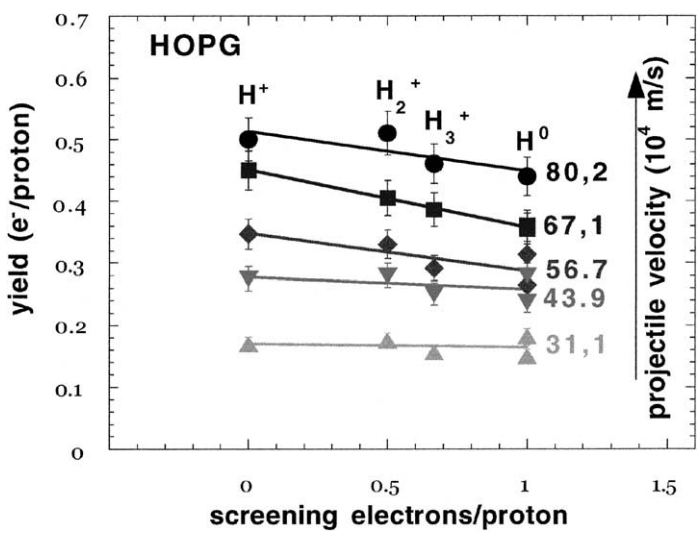

Fig. 8. Measured electron yields per proton for impact of atomic and molecular hydrogen projectiles on clean graphite plotted as a function of the number of screening electrons per proton at different projectile velocities. Yields for hydrogen atoms H^0 were derived from data for impact of protons and $H_2{}^+$ or protons and $H_3{}^+$, respectively by using Eq. (2).

confidence that Eq. (1) can also be applied to molecular hydrogen ions on graphite (as in the case of Au). As a result we find that hydrogen atoms liberate about 10% less electrons than equally fast protons.

For discussion of our results we will consider the different mechanisms for electron emission and therefore concentrate on KE only since PE due to Auger neutralization [23,24] can be neglected for the singly charged ion species applied here. In conducting targets the most prominent KE mechanism (at least for sufficiently fast projectiles) is momentum transfer in collisions of the projectile with quasi-free metal electrons ("eKE process") [9,25]. In such collisions, however, quasi-free electrons from the Fermi gas can only be ejected into vacuum above the so-called "classical threshold" impact velocity $v_{\mathrm{th,e}}$ which depends on the respective work function W_ϕ, and also on the Fermi velocity v_F (Fermi energy E_F) of the electrons in the solid [9,25–28] according to Eq. (3).

$$v_{\mathrm{th,e}} = \frac{1}{2} v_\mathrm{F} \left(\sqrt{1 + \frac{W_\phi}{E_\mathrm{F}}} - 1 \right) \tag{3}$$

While the work functions are almost the same for Au and graphite, their Fermi energies are quite different (see Fig. 9).

This results in an accordingly different value for the "classical threshold" velocity ($v_{\mathrm{th,e}}(\mathrm{Au}) \approx 2.4 \times 10^5$ m/s or ca. 300 eV/amu; $v_{\mathrm{th,e}}(\mathrm{C}) \approx 1.5 \times 10^5$ m/s or ca. 120 eV/amu). Experimentally, we observe a correct trend but in a qualitative way only (i.e., $v_{\mathrm{th,e}}(\mathrm{C}) < v_{\mathrm{th,e}}(\mathrm{Au})$). With measured $v_{\mathrm{th,e}}(\mathrm{Au}) \approx 3.4 \times 10^5$ m/s, electron emission from Au requires higher impact velocities than predicted by Eq. (3), while for the carbon target electron emission already starts at $v_{\mathrm{th,e}}(\mathrm{C}) \approx 1.0 \times 10^5$ m/s and thus is clearly lower than calculated by Eq. (3). This points to the importance of other KE mechanisms like electron promotion into continuum in projectile collisions with individual target atoms [28,29] and/or a newly proposed "surface-assisted KE" process [30]. Recent calculation, indeed shows that surface-assisted KE can explain both the energy dependence and magnitude of the observed electron yields quite well [31]. The reasons for the observed difference between results for HC- and LC-oriented

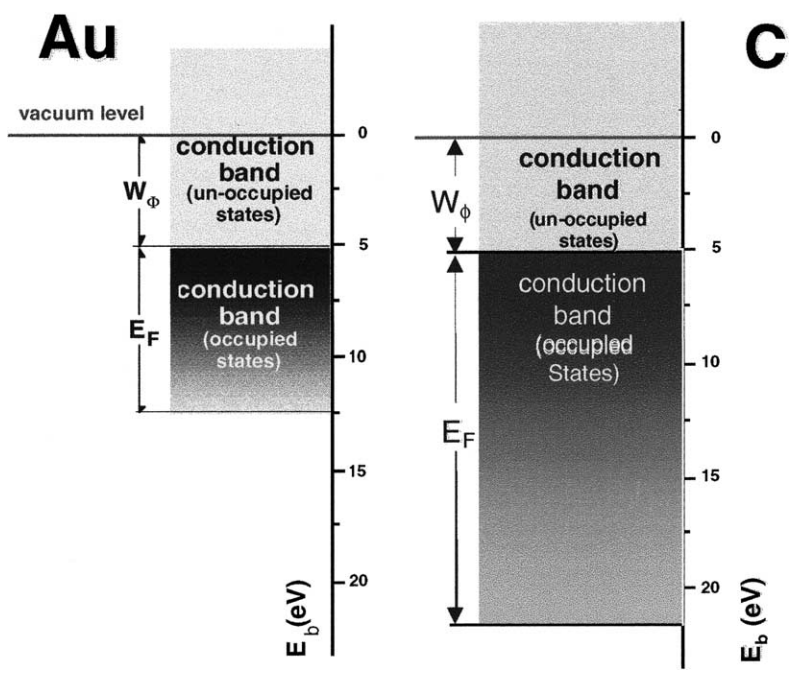

Fig. 9. C and Au targets feature similar work function but rather different Fermi energies.

carbon tiles can, however, only be speculated upon. It could, for example, be either due to differences in projectile penetration and stopping power or to preferred directions for electron transport.

2.5. Results for multiply charged projectiles

So far only preliminary results have been obtained with MCIs. Fig. 10 shows measured total electron yields γ induced by impact of C^+, C^{2+}, C^{4+} and C^{5+} ions on carbon tiles (C_L only) as well as on HOPG. The electron yield strongly increases with projectile charge state which can be attributed to potential electron emission (PE) [32]. Since PE has no impact energy threshold [33], electrons can be emitted already at impact energies of a few eV only.

This might have consequences for the sheath potential (cf. Discussion in Chapter 4) and we will therefore continue our studies for other MCI species like O^{q+} and Ne^{q+} which are also of relevance in the edge region of fusion plasmas (oxygen being an almost unavoidable intrinsic impurity and neon being sometimes injected for modifying the edge plasma temperature profile via enhanced radiation cooling).

3. Fragmentation of molecular ions

3.1. Reactive interactions of molecular ions with surfaces

Ion–surface (reactive) collisions is a research area which is rapidly growing in an effort to identify and explore new methods for characterizing gaseous ions and the nature of the surface and for elucidating plasma–wall interaction phenomena. Besides physical and chemical sputtering the following processes have been identified and investigated in the past years for collisions in the range of tens of eV laboratory energy:

1. reflection,
2. surface-induced dissociation (SID),
3. charge exchange reactions (CER) and
4. surface-induced reactions (SIR).

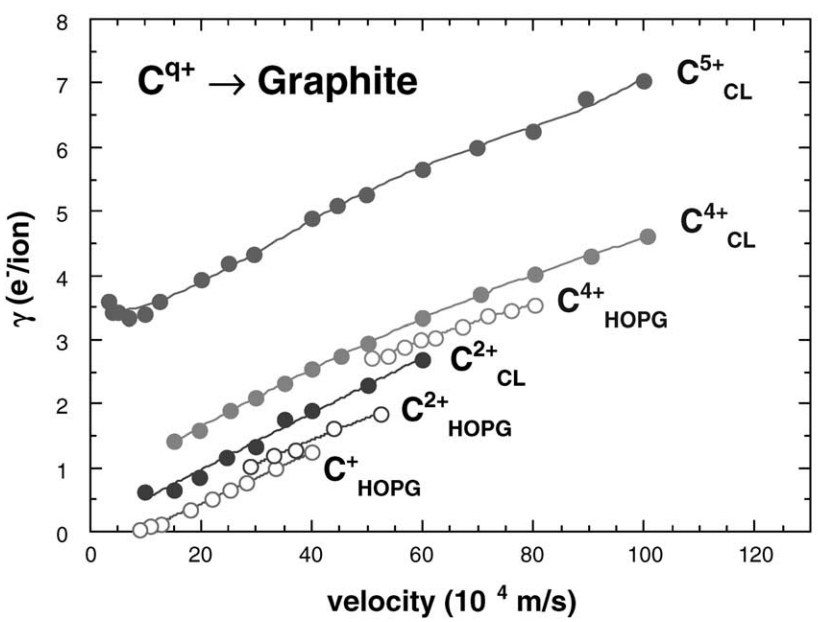

Fig. 10. Total electron yields vs. impact velocity v for impact of C^+, C^{2+}, C^{4+} and C^{5+} ions on carbon tiles (C_L only) and HOPG.

These four reactions may be written schematically for a primary projectile ion m_1^+ or m_1^{2+} colliding with a surface *S* being covered with an adsorbate AB in the following way, respectively:

$$m_1^+ \rightarrow \frac{S}{AB} \rightarrow m_1^+ \text{ or } m_1^{*+} \quad (4)$$

$$m_1^+ \rightarrow \frac{S}{AB} \rightarrow m_1^{*+} \rightarrow m_2^+ + m_3 \quad (5)$$

$$m_1^{2+} \rightarrow \frac{S}{AB} \rightarrow m_1^{*+} \rightarrow m_2^+ + m_3 \quad (6)$$

$$m_1^+ \rightarrow \frac{S}{AB} \rightarrow m_1AB^{*+} \text{ or } m_1A^{*+} \quad (7)$$

In addition to being of fundamental importance, polyatomic ion–surface reactions are also relevant to technological applications encompassing such diverse fields as: (i) secondary ion mass spectrometry; (ii) reactive scattering for surface analysis; (iii) surface-induced dissociation for structural analysis; (iv) surface modifications for the preparation of new electronic materials (including the large area of plasma processing) and, quite importantly in the present context; (v) plasma–wall interactions in electrical discharges and fusion plasmas [4,8].

Typically, polyatomic ion–surface reactions are studied with a tandem mass spectrometer set-up consisting of a combination of two or more mass analyzers such as a magnetic sector field analyzer (B), a quadrupole mass analyzer (Q) or a time-of-flight (TOF) analyzer [34–37]. The first mass analyzer is used to select the primary ion and the second mass analyzer (sometimes complemented by an energy analyzer) is employed to record the secondary mass spectrum as a function of the collision energy (and sometimes as a function of energy and angle). In order to allow a quantitative investigation of SID and SIR processes it is important to control and determine accurately the collision energy and to achieve energy spreads as small as possible. So far the best energy resolution achieved for the study of polyatomic ions was a FWHM distribution of about 2–4 eV [38]. In a recent effort to improve this situation we have constructed the tandem mass spectrometer set-up BESTOF (consisting of a B-sector field combined with an E-sector field, a surface and a time-of-flight mass spectrometer) [37,39,40] which allows the investigation of ion–surface reactions with high primary mass and energy resolution, i.e., energy spreads of as low as 80 meV FWHM have been achieved. In the following we will first describe the characteristics and the performance of this newly constructed tandem mass spectrometer system BESTOF. We will then discuss in an illustrative manner results obtained with this machine selecting as an example the same projectile/surface system (i.e., H_2^+ and H_3^+ colliding with graphite tiles from the Tokamak experiment Tore Supra from Cadarache) as discussed above for the electron emission studies.

3.2. Experimental set-up and technique

The experimental apparatus BESTOF (see Fig. 11) constructed recently in Innsbruck [37,39,40] consists of a double focusing two-sector field mass spectrometer (reversed geometry) in combination with a linear TOF mass spectrometer. Projectile ions to be used after proper mass and energy analysis may be produced in a variety of ways including a Nier type electron impact ion source, a supersonic expansion cluster source, a pulsed arc cluster ion source, a Colutron gas discharge source or an electron cyclotron resonance ion source. For the present investigations we used a recently commissioned Colutron low-pressure DC gas discharge ion source allowing us to produce the required projectile ions in abundant intensities.

The ions produced in the Colutron ion source are extracted/focussed from the ion source region and accelerated to about 3 keV for mass- and energy-analysis by the double-focusing two-sector field mass spectrometer. The nominal mass resolution of this two-sector field mass spectrometer exceeds at 3 keV a value of 10,000 and thus allows easily for selection of isotopically pure primary ions. Fig. 12 shows as an example a primary mass spectrum obtained by operating the Colutron ion source with a 9:1 mixture of H_2 and CH_4.

After passing the exit slit of the mass spectrometer, ions are refocused by an Einzel lens and the deceleration optics positioned in front of the stainless steel

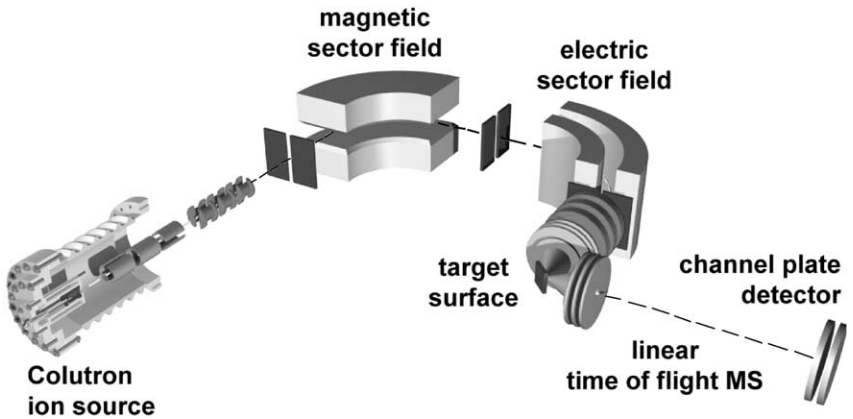

Fig. 11. Schematic view of the experimental apparatus BESTOF combined with a Colutron ion source.

surface. Field penetration effects are minimized by shielding the surface with conical shield plates. The incident impact angle δ of the primary ions at the surface is usually kept at 45° and the scattering angle is fixed at 91°. The collision energy of ions impacting on the surface is defined by the potential difference between the ion source and the surface. The potential difference (hence, the collision energy) can be varied from 0 to about 2 keV. We have determined the energy and energy spread of the primary ion beam by using the surface as a retarding potential and measuring the (reflected) total ion signal as a function of the surface potential. The energy spread is given by the FWHM of the first derivative of the total ion signal. Fig. 13 shows as an example the total reflected ion current for the impact of the molecular hydrogen ion H_2^+ as a function of the nominal retarding potential in the vicinity of the ion acceleration potential of approximately 2929 V. If the retarding potential is above the acceleration potential, no ions will hit the surface and thus no ions will be detected, and if the retarding potential is lowered, primary ions will start to be

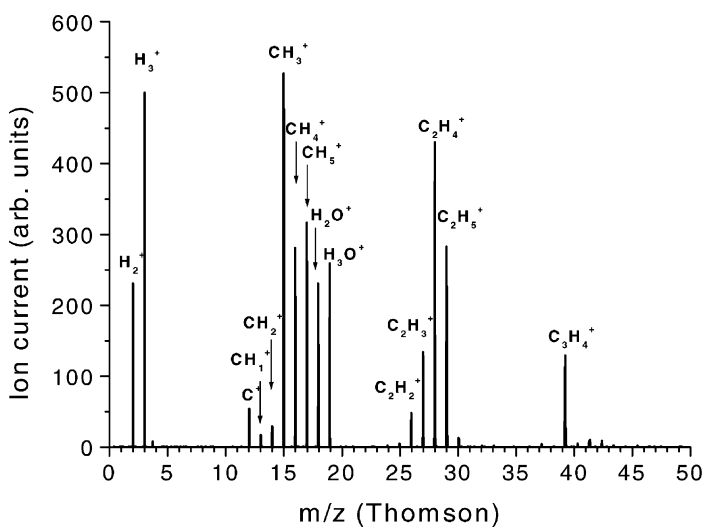

Fig. 12. Primary ion mass spectrum for a 9:1 H_2/CH_4 gas mixture in the Colutron ion source. Corresponding primary ions are identified.

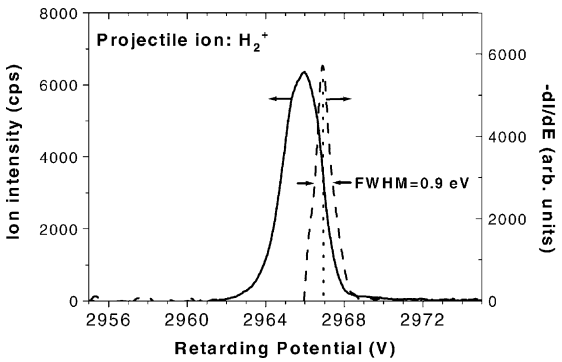

Fig. 13. Total reflected ion current, solid curve, for the surface impact of H_2^+ ions as a function of the nominal retarding potential in the vicinity of the ion acceleration potential of approximately 2967 V. The derivative of the leading edge of the total reflected ion current I with respect to the energy E, shown by dashed curve, indicates a FWHM for the primary ion beam of about 0.9 eV.

able to hit the surface and the reflected ion current will strongly increase to its peak value. The ensuing decrease of the reflected ion current with decreasing retarding potential (increasing collision energy) is due to the loss of primary ions at the surface via neutralization processes. The derivative of the leading edge of this total reflected ion current also shown in Fig. 13 indicates, in this case, a FWHM for the primary ion beam spread of about 0.9 eV. This energy spread is caused by the ion production process and the ion extraction from the Colutron ion source (similar energy spreads have been measured for other ions from this source) and is somewhat larger than the typical energy spread of about 100–200 meV which can be achieved with ions from a Nier type ion source [37].

A fraction of the secondary ions formed at the surface exits the shielded chamber through a 1 mm diameter orifice. These ions are then subjected to the pulsed extraction and acceleration field which initiates TOF analysis of these ions. This second mass analyzer is a linear TOF mass selector with a flight tube of about 80 cm in length. The mass selected ions are detected by a double stage multi-channel plate which is connected to a fast scaler (with a time resolution of 5 ns per channel) and a laboratory computer. Mass resolution has been improved steadily in the past 2 years and is to date approximately 100.

In the initial stage of our present studies, experiments have been carried out using a stainless steel surface under ultra high vacuum conditions (10^{-10} Torr) maintained in our bakeable turbo-pumped surface collision chamber. However, even these conditions do not exclude the production of monolayers of hydrocarbon contaminants (pump oil, etc.) on the surface whenever the valve between the mass spectrometers and the surface collision chamber is opened and the pressure in the target region is rising to the 10^{-9} Torr range.

3.3. Results for H_2^+ and H_3^+ projectile ions

In a first check about the reliability of the present machine after installing the new Colutron ion source, we have repeated some of the earlier ion–surface collision-induced dissociation and collision-induced reaction measurements [37,39,40] thereby proving the correct working condition of the whole set-up. In a next step we proceeded to the study of the most basic molecular ion–surface interaction involving the simple hydrogen ions H_2^+ and H_3^+. These measurements were first carried out for comparison with earlier studies and standardization with stainless steel and HOPG surfaces and then with fusion-relevant carbon-based materials, i.e., using the same carbon tile samples from Tore Supra as described in Chapter 2. The surface samples have been studied (i) either ‘as is’ under the vacuum conditions present in our machine (10^{-10} Torr), in which case the surface is assumed to be covered with adsorbed gases from the background or (ii) after cleaning the surface with an ion sputter gun. In each case we have not only measured the total reflected ion current, but also performed mass analysis of the product ions being produced by the impact of the projectile ions. Furthermore, the reactive interactions have been studied as a function of collision energy (thus yielding energy resolved mass spectra, ERMS) up to an energy of about 200 eV (see details as follows).

As mentioned in Section 1, so far laboratory studies in the frame of fusion oriented investigations concerning reactive interactions in the low energy regime below 200 eV have been limited, i.e., involving only

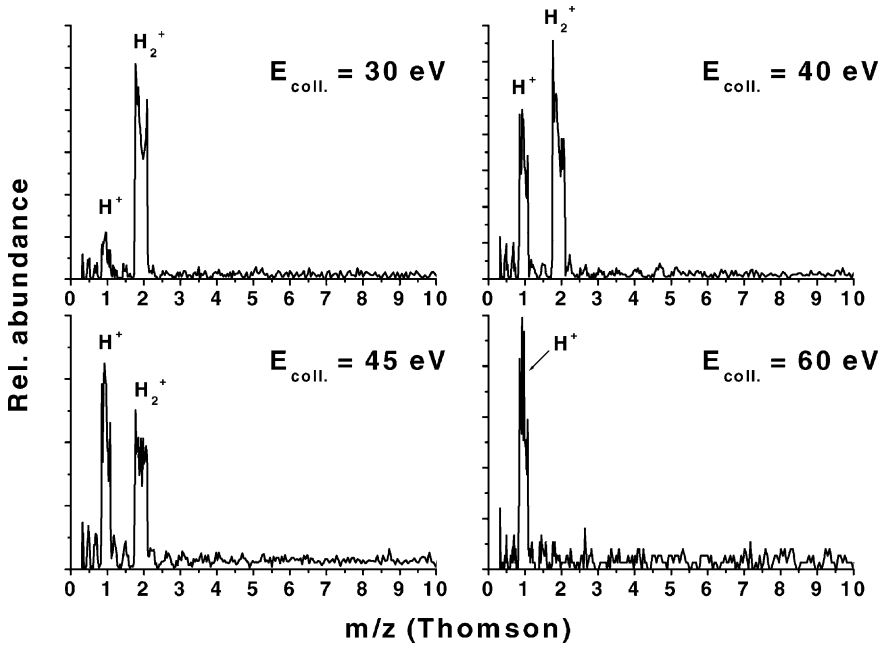

Fig. 14. Secondary ion mass spectra after impact of H_2^+ with different collision energies on a carbon tile sample covered by hydrocarbons.

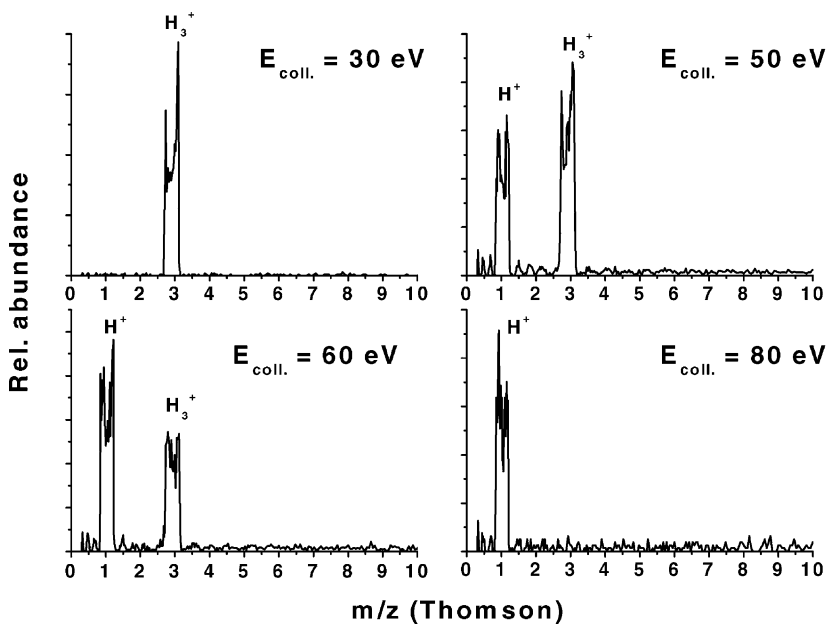

Fig. 15. Secondary ion mass spectra after impact of H_3^+ with different collision energies on a carbon tile sample covered by hydrocarbons.

H^+ and O^+ projectiles ions. Here we have extended these studies to molecular hydrogen ions for the first time including in a systematic fashion the species H_2^+, and H_3^+. Possible dissociation pathways and its concomitant energetics [41] for these ions are listed as follows:

$$H_2^+ \Rightarrow H^+ + H \quad (2.69\,eV) \tag{8}$$

$$H_3^+ \Rightarrow H^+ + H_2 \quad (4.39\,eV) \tag{9}$$

$$H_3^+ \Rightarrow H_2^+ + H \quad (6.22\,eV) \tag{10}$$

$$H_3^+ \Rightarrow H^+ + H + H \quad (8.91\,eV) \tag{11}$$

As can be seen from Figs. 14 and 15, which show as an example secondary mass spectra for the H_2^+ and H_3^+ ion, respectively, at some selected collision energies, also in the case of the triatomic projectile ion quite unexpectedly the only fragment ion to be observed is the atomic ion. This is in line with the energetics shown above which demonstrate that production of the proton plus one neutral H_2 is the energetically favored reaction.

In Figs. 16 and 17 the present measurements concerning the H_2^+ and H_3^+ ions interacting with stainless steel and Tore Supra carbon tile surfaces are summarized in form of ERMS plots. As a matter of fact, due to the surprising results obtained we have repeated all of these measurements several times and under different experimental conditions.

Several trends can be deduced from the results shown in Figs. 16 and 17.

Both the diatomic and the triatomic hydrogen molecular projectile ions (H_2^+ and H_3^+) fragment exclusively into the atomic counterparts. This is in accordance with results concerning the angular dependence of backscattering of keV molecular ions studied by Eckstein et al. [42] and photofragmentation of these molecular ions by Carrington and Kennedy [43].

The fragmentation patterns are very similar for the two target surfaces.

The threshold values and the 50% crossing point values occur at higher energies for the heavier molecular ion, i.e., 26.8 and 29.3 eV or 44 and 55 eV, respectively (see Fig. 16), when going from the H_2^+ to the

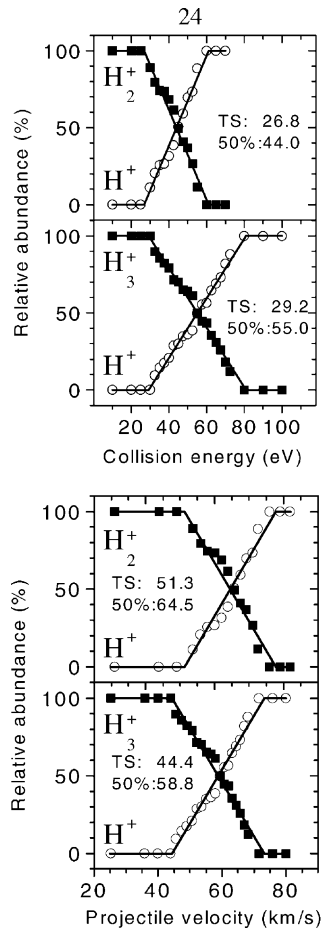

Fig. 16. Energy resolved mass spectrum (ERMS) plot (upper panel) and velocity resolved mass spectrum (VRMS) plot (lower panel) for the interaction of the H_2^+ and H_3^+ with a stainless steel surface covered with hydrocarbons. TS: threshold energy (velocity) in eV; 50%: energy (velocity) at crossing point in eV.

H_3^+ case. This is in accordance with the somewhat larger binding energy of the H^+ ion in the triatomic ion as compared to the diatomic case (see Eqs. (8) and (9)). It is interesting to note that the threshold energies are shifted by about the same order of magnitude as the different binding energies (approximately 2 eV), whereas the 50% crossing point is shifted by a much larger amount (approximately 10 eV).

Finally, when the data are converted from an ERMS type plot to a VRMS type plot the ordering in the

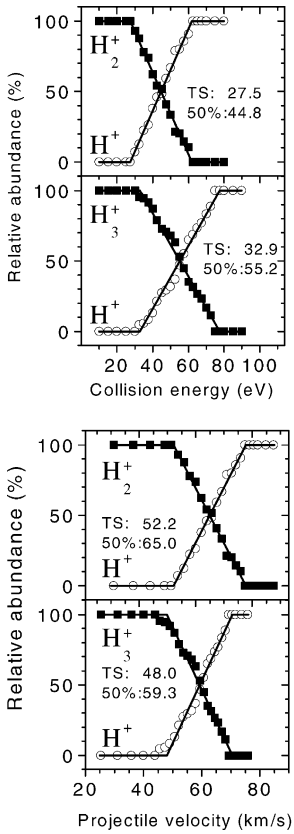

Fig. 17. Energy resolved mass spectrum (ERMS) plot (upper panel) and velocity resolved mass spectrum (VRMS) plot (lower panel) for the interaction of the H_2^+ and H_3^+ with a graphite surface of a Tore Supra tile from Cadarache. TS: threshold energy (velocity) in eV; 50%: energy (velocity) at crossing point in eV.

threshold value and the crossing point value is changing drastically.

It is interesting to note that we have recently also started to use deuterated projectile ions [44], thus allowing us to obtain information about H-retention (see Discussion in [45]). These studies will give us information concerning the relative importance of charge exchange reactions as compared to dissociation reactions and pick up reactions when analysing the ERMS spectra obtained. It is clear that the outcome of these ion–surface collisions in terms of the different reaction products will crucially influence the composition of the plasma in the plasma edge and may also be of importance in the H-retention process.

4. Implications of the results for plasma edge modelling

In order to demonstrate the importance of the present results we will discuss as an illustrative example the influence of electron emission on the sheath potential.

4.1. Electron-induced electron emission

The role of electron (re-)emission and its influence on the sheath potential has been treated by various authors [46–52]. The normalized sheath potential ψ_s in the presence of (electron-induced) electron emission is given by [53]

$$\psi_s = \frac{eV_s}{kT_e} = -\frac{1}{2}\ln\left\{\frac{2\pi m_e(1+T_e/T_i)}{m_i(1-\gamma)^2}\right\} \quad (12)$$

where m_i, m_e, T_i and T_e are the ion and electron masses and temperatures, respectively and γ denotes the secondary emission yield. In the absence of space charge the sheath potential for a pure hydrogen plasma drops to 0 at around $\gamma = 0.92$ [46,48], a value typically reached for 200–300 eV electrons on graphite surfaces at incidence angles >60° with respect to the surface normal [48]. However, in the scrape-off layer (SOL) plasma of toroidal fusion devices with magnetic divertors, magnetic field lines usually connect to the target plates at grazing incidence. On the other hand, the electron gyromotion around these grazingly incident magnetic field lines tend to suppress electron emission [49]. The relevance of this effect again depends on the strength of the electric field across the plasma sheath that accelerates the emitted electrons away from the target surface, which calls for more detailed simulation calculations.

4.2. Singly charged ion-induced electron emission

As seen from the data presented in Section 2.1, electron emission induced by impact of singly charged ions on carbon targets only starts at an impact energy of about 50 eV/amu. At typical sheath potentials of 200 V the total electron yield even for the light hydrogen ions

is still rather small (typically 0.2 electrons/ion) if compared to the electron-induced emission yield. Singly charged ion-induced electron emission is therefore usually neglected in plasma simulation codes. However, ion-induced kinetic electron emission exhibits an impact angle Θ dependence of approximately $\gamma(\Theta) \approx \gamma_0 \cos^{-1}(\Theta)$ [9], which means that under grazing angles of incidence the yields may become much larger. A more definite answer for the role of (singly charged) ion-induced electron emission can only be gained from more complex simulation calculations.

4.3. Multiply charged ion-induced electron emission

The electron yield for MCIs strongly increases with the projectile charge state q of the ion [32]. Moreover, the mainly responsible mechanism (potential electron emission) has no impact energy threshold, which means a considerable number of electrons can be emitted even at quite low impact energies. On the other hand, MCIs due to their charge are accelerated by the sheath potential to higher impact energies (qV_s) as compared to singly charged ions (several keV instead of several 100 eV), which further increases the electron emission yield due to an increasing importance of kinetic electron emission (see Fig. 10). To exert an influence on the sheath structure, the flux of electrons emitted due to MCIs has to be a substantial fraction of the total number of emitted electrons. According to an estimate presented by Lackner and Schweinzer [54] under the assumption of a maximum $Z_{\text{eff}} = 2$, a related influence of MCI-induced electron emission can be expected if $\gamma \approx Z$. This condition is certainly met if one considers our results presented in Fig. 10.

Again simulation calculations, by e.g., using a particle-in-cell code, would be highly desirable to determine the conditions under which particle-induced electron emission could attain a non-negligible influence on the edge plasma conditions.

Acknowledgements

This work has been carried out within Association EURATOM—ÖAW. The content of the publication is the sole responsibility of its publishers and it does not necessarily represent the views of the EU Commission or its services. Work was partially supported by the FWF and the ÖAW, Wien, Austria and the European Commission, Brussels. It is a pleasure to thank Dr. W. Hess from Association EURATOM—CEA, Cadarache, for supplying the presently used graphite tiles from the Tokamak experiment Tore Supra.

References

[1] J. Roth, K. Ertl, C. Linsmeier (Eds.), Plasma-surface Interactions in Controlled Fusion Devices-14 J. Nucl. Mater. 290–293 (2001).
[2] P.C. Stangeby, G.M. McCracken, Nucl. Fusion 30 (1990) 1225.
[3] E.W. Thomas, ORNL, Atomic Data for Controlled Fusion Research, 1985.
[4] W.O. Hofer, J. Roth, Physical Processes of the Interaction of Fusion Plasmas with Solids, Academic Press, San Diego, 1996.
[5] E. Vietzke, A.A. Haasz, in: W.O. Hofer, J. Roth (Eds.), Physical Processes of the Interaction of Fusion Plasmas with Solids, Academic Press, San Diego, 1996 (Chapter 4).
[6] H. Sugai, Y. Mitsuoka, H. Toyoda, J. Vac. Sci. Technol. A16 (1998) 290.
[7] C. Mair, H. Deutsch, K. Becker, M. Lezius, T.D. Märk, E. Vietzke, W.R. Hess, in: Proceedings of the 27th EPS Conference, Budapest, 2000.
[8] R.K. Janev, Atomic and Molecular Processes in Fusion Edge Plasma, Plenum Press, New York, 1995.
[9] D. Hasselkamp, in: G. Höhler (Ed.), Particle-Induced Electron Emission II, Vol. 123, Springer, Heidelberg, 1992, p. 1.
[10] H. Kurz, K. Töglhofer, HP. Winter, F. Aumayr, R. Mann, Phys. Rev. Lett. 69 (1992) 1140.
[11] F. Aumayr, H. Kurz, D. Schneider, M.A. Briere, J.W. McDonald, C.E. Cunningham, HP. Winter, Phys. Rev. Lett. 71 (1993) 1943.
[12] C. Lemell, J. Stöckl, J. Burgdörfer, G. Betz, HP. Winter, F. Aumayr, Phys. Rev. Lett. 81 (1998) 1965.
[13] H. Eder, F. Aumayr, HP. Winter, Nucl. Instrum. Meth. B 154 (1999) 185.
[14] A. Shirley, Phys. Rev. B 5 (1972) 4709.
[15] U. Fleck, H. Wann, P. Ziesche, Phys. Status Solidi 61 (1980) 447.
[16] P.M. Echenique, R.M. Nieminen, J.C. Ashley, R.H. Ritchie, Phys. Rev. A 33 (1986) 897.
[17] M. Leitner, D. Wutte, J. Brandstötter, F. Aumayr, HP. Winter, Rev. Sci. Instrum. 65 (1994) 1091.
[18] H. Eder, W. Messerschmidt, HP. Winter, F. Aumayr, J. Appl. Phys. 87 (2000) 8198.
[19] L.N. Large, W.S. Whitlock, Proc. Phys. Soc. London 79 (1962) 148.

[20] E.R. Cawthron, Aust. J. Phys. 24 (1971) 859.
[21] S.M. Ritzau, R.A. Baragiola, Phys. Rev. B 58 (1998) 2529.
[22] G. Lakits, F. Aumayr, HP. Winter, Europhys. Lett. 10 (1989) 679.
[23] H.D. Hagstrum, Phys. Rev. 96 (1954) 325.
[24] H.D. Hagstrum, Phys. Rev. 96 (1954) 336.
[25] R.A. Baragiola, E.V. Alonso, A. Olivia-Florio, Phys. Rev. B 19 (1979) 121.
[26] G. Lakits, F. Aumayr, M. Heim, HP. Winter, Phys. Rev. A 42 (1990) 5780.
[27] M. Rösler, W. Brauer, in: G. Höhler (Ed.), Particle-Induced Electron Emission I, Vol. 122, Springer, Berlin, 1991.
[28] R. Baragiola, in: J.W. Rabalais (Ed.), Low energy Ion–Surface Interactions, Wiley, New York, 1993 (Chapter 4).
[29] U. Fano, W. Lichten, Phys. Rev. Lett. 14 (1965) 627.
[30] J. Lörincik, Z. Sroubek, H. Eder, F. Aumayr, HP. Winter, Phys. Rev. B 62 (2000) 16116.
[31] J. Lörincik, Z. Sroubek, S. Cernusca, A. Diem, HP. Winter, F. Aumayr, Surf. Sci. 504 (2002) 59.
[32] HP. Winter, F. Aumayr, J. Phys. B: Atom. Mol. Opt. Phys. 32 (1999) R39.
[33] A. Arnau, et al., Surf. Sci. Reports 229 (1997) 1.
[34] R.G. Cooks, T. Ast, M.A. Mabud, Int. J. Mass Spectrom. Ion Process. 100 (1990) 209.
[35] A. Amirav, Comm. Atom. Mol. Phys. 24 (1990) 187.
[36] L. Hanley (Ed.), Special Issue of Int. J. Mass Spectrom. 174 (1998).
[37] C. Mair, T. Fiegele, F. Biasioli, R. Wörgötter, V. Grill, T.D. Märk, Plasma Sources Sci. Technol. 8 (1999) 191.
[38] S.B. Wainhaus, E.A. Gislason, L. Hanley, J. Am. Chem. Soc. 119 (1997) 4001.
[39] V. Grill, R. Wörgötter, J.H. Futrell, T.D. Märk, Z. Phys. D 40 (1997) 111.
[40] C. Mair, T. Fiegele, R. Wörgötter, J.H. Futrell, T.D. Märk, Int. J. Mass Spectrom. Ion Process. 177 (1998) 105.
[41] J.L. Franklin, J.G. Dillard, H.M. Rosenstock, J.T. Herron, K. Draxl, F.H. Field, Ionization Potentials, Appearance Potentials and Heat of Formation of Gaseous Positive Ions, National Bureau of Standards, USA, NSRDS-NBS 26, 1969.
[42] W. Eckstein, H. Verbeek, S. Datz, Appl. Phys. Lett. 27 (1975) 527.
[43] A. Carrington, R. Kennedy, J. Chem. Phys. 81 (1984) 91.
[44] A. Qayyum, W. Schustereder, C. Mair, Z. Herman, W.R. Hess, P. Scheier, T.D. Märk, in: Proceedings of the 13th Symposium on Atomic and Plasma Physics, Going, 2002.
[45] G. Federici, J. Nucl. Mater. 266 (1999) 14.
[46] J.N. Brooks, J. Nucl. Mater. 93/94 (1980) 437.
[47] W.O. Hofer, J. Vac. Sci. Technol. A 5 (1987) 2213.
[48] J.M. Pedgley, G.M. McCracken, Plasma Phys. Contr. Fusion 35 (1993) 397.
[49] S. Takamura, S. Mizoshita, N. Ohnu, Phys. Plasmas 3 (1996) 4310.
[50] W.X. Wang, M. Okamoto, N. Nakajima, S. Murakami, N. Ohyabu, Nucl. Fusion 37 (1997) 1145.
[51] K. Ohya, Nucl. Instrum. Meth. Phys. Res. B 153 (1999) 58.
[52] I.V. Tsvetkov, T. Tanabe, J. Nucl. Mater. 266–269 (1999) 714.
[53] P.C. Stangeby, in: D.E. Post, R. Behrisch (Eds.), Physics of Plasma Wall Interactions in Controlled Fusion, Plenum Press, New York, 1986, p. 41.
[54] K. Lackner, J. Schweinzer, Private communication, 1996.